Negative Differential Conductance Materials for Flexible Electronics

Alain Nogaret

Department of Physics, University of Bath, Claverton Down, Bath BA2 7AY, UK

Correspondence to: Alain Nogaret (E-mail: *A.R.Nogaret@bath.ac.uk*)

ABSTRACT

The need for electronics that is compatible with life is driving the search for electronically active materials that may be used for transferring integrated circuits onto flexible substrates. One route is to build transistors which modulate the conductivity of organic thin films with a lateral gate. However, as is well known in the case of graphene, the in-plane conductivity cannot easily be switched off. Another route is to use negative differential resistance (NDR) phenomena. Until recently, NDR was only obtained from band engineered semiconductors. This paper reviews the recent development of flexible materials that specifically make use of transport perpendicular to graphite planes to obtain NDR. These materials include h-boron-nitride/graphene multilayers and graphite-silicone composites. We report on the dependence of their current-voltage curves on deformation, changes in structural and experimental parameters. We also describe device implementations in the form of flexible oscillators, amplifiers and memories.

KEYWORDS Graphite-silicone composite, Flexible electronics, Negative differential resistance, Pressure sensing, Mechanoreceptors.

AUTHOR BIOGRAPHIES

Dr Alain Nogaret was awarded a PhD in Physics on the magneto-tunneling spectroscopy of III-V semiconductor multilayers. He currently studies negative differential resistance in graphitic compounds and spin dynamics in magnetically modulated two-dimensional electron systems. He has demonstrated robust negative differential resistance in flexible composites which he uses to make flexible amplifiers and strain sensors. He has also demonstrated commensurability oscillations in lateral magnetic superlattices, channeling by magnetic edge states and electrically induced spin resonance.

1. INTRODUCTION

For decades the miniaturization of transistor circuitry has underpinned progress in electronics. Increases in integration density have brought gains in speed and memory capacity while dramatically reducing power consumption. The latter has dropped by 4 orders of magnitude from 0.4μJ per floating point operation (flop) in 1997 to 70pJ in 2012. Although the scaling down of integrated circuits has been predicted to reach its physical limits for many years, technological prowess, notably the development of high permittivity dielectrics, has enabled the scaling of transistor gates to dimensions as small as 22nm. Over the next decade, energy requirements are forecast to drop to 5-10pJ per flop. In parallel with the miniaturization in silicone chips, novel materials have been sought to build integrated circuits on flexible substrates.[1,2] This effort is motivated by the need for ergonomic human-computer interfaces that fit the human body, curved surfaces and moving parts. Applications areas include conformable displays,[3-8] touch sensitive pads,[9-13] Braille displays,[14] body wearable sensors,[15,16] medical probes and implants,[17-19] artificial retinas,[20,21] and artificial skins.[22,19, 23-25] As most flexible materials are electrical insulators, attention has focused on conjugated polymers that allow electron to delocalize along molecular chains and hop from one molecule to another. These polymers tend to have p-type conduction[26] which hinders the realization of CMOS logic. Recently electric field induced ambipolar conduction has also been achieved.[27,28] Organic polymers are prone to decay under bias voltage cycling and oxidation at the site of the conjugated bonds. The development of organic thin films for transistors,[26,28] molecular electronics[29] and organic electro-luminescent devices has already been covered in excellent reviews.[29-31]

The purpose of this review is to report on novel graphitic compounds that exhibit NDR in their current-voltage (I-V) curves. These materials combine electronically active properties with the ability to bend. The NDR is a region of the I-V curves where the current decreases ($\Delta I < 0$) when the bias voltage increases ($\Delta V > 0$). The negative differential conductance $g = \Delta I / \Delta V$ is the figure of merit that defines active properties such as the voltage and power gain.[32] Here, we describe the synthesis of these materials and the physical mechanisms underpinning the NDR as these differ from quantum mechanical tunneling in band engineered semiconductors. We show how NDR devices achieve the traditional functions of transistors such as voltage amplification,[32] bistable memories and are unique in implementing multilevel logic[33] and high frequency generation.[34,35] The recent demonstration of NDR in flexible materials opens an exciting new direction for fundamental research on the coupling between mechanical deformation and electronic gain which opens a range of new possibilities for electromechanical sensing.[36,37]

Table I shows the main families of devices fabricated on rigid and flexible substrates. Field effect transistors and opto-electronic devices have already been translated from silicon or III-V semiconductors to organic thin films. In contrast, NDR devices such as Esaki diodes, double barrier resonant tunneling structures and superlattices have only been implemented on crystalline substrates. These devices require band engineered semiconductor structures which are modulated on the atomic scale and are defect free in order to produce a tunneling current which decreases with increasing voltage. These are stringent conditions for organic thin films which are not easily structured at the supramolecular level. The present paper reports on the observation of tunneling NDR in flexible graphitic compounds which combine long range atomic order with flexibility. These are the graphene-boron nitride[38] and graphite-silicone[39] systems in which a current may be injected perpendicular to the atomically thin graphite planes.

From a technological point of view, one may ask what benefit would the novel graphitic structures confer to NDR devices given that semiconductor NDR has so far only supplanted transistors in niche application such as high frequency mixing.[35] In fact, perpendicular transport through graphene planes presents many advantages over semiconductor multilayers. In III-V tunneling structures, quantum resonances and the associated NDR have been blurred by the thermionic current component activated over the tunneling barriers. These problems have been addressed by using materials with higher tunneling barriers such as boron nitride,[38] or polysilane[39] to quench the thermionic current. *Secondly*, the tunneling process leading to NDR in graphitic compound is very robust as it does not involve resonance through a localized energy level bound to quantum well. Further, the peak-to–valley current ratio - which measures the switching contrast - can theoretically be infinite[39] unlike in semiconductor multilayers. *Thirdly*, the graphene-boron nitride tunneling system has both atomically thin graphene electrodes and boron-nitride barriers which allows atomic level miniaturization.[38] *Fourthly*, graphene boron-nitride trilayers have negligible transit times due to the absence of a central quantum well. As a result, one expects faster response time than in resonant tunneling structures where Fabry-Perot type resonances impose a dwell time of a few picoseconds. Boron-nitride trilayers could thus operate as quasi-optical sources at generating frequencies in excess of the THz. *Fifth*, the flexibility of graphitic materials has allowed the voltage oscillations generated by the NDR region to be tuned by strain. In this way the NDR material mimics the response of biological mechanoreceptors and opens a new route towards accurate pressure sensing. The conversion of strain into voltage oscillations of frequency proportional to strain replicates the response of electromechanical sensors (Merkel cells)[40,41] in the skin. The coding of strain into frequency is believed to explain the high sensitivity of the human touch.

Perpendicular transport presents an attractive alternative to in-plane transport in graphene as the lack of energy band gap makes it difficult to turn off the in-plane conduction through the action on an electrostatic gate. By contrast, perpendicular transport in graphitic compounds has already obtained amplification gain, electromechanical sensing and offers high peak-to-valley current ratios with the real prospects of material improvement in the near future.

TABLE 1 Rigid and flexible electronics.

	Transistors	**NDR devices**	**Opto-electronics**
Rigid substrates	Field effect transistors Bipolar transistors	Esaki diodes Semiconductor superlattices Resonant tunneling diodes	Light Emitting Diodes Optocouplers, LASER heterojunctions
Flexible substrates	Organic transistors	→ **THIS REVIEW** ←	Organic electroluminescent devices

The paper is organized as follows. Section 1 presents the background and motivations; Section 2 reviews the science and technology of transistors and electro-luminescent devices made from flexible materials as well as the routes towards their synthesis; Section 3 covers the materials for NDR including semiconductors, metal-organic thin films, graphene-boron-nitride trilayers and graphite-silicone composites; Section 4 describes the behavior of the NDR under strain and the analogy with mechanoreceptors in the human skin; Section 5 describes demonstrates voltage amplification by plastic materials and proposes simple multilevel memories; the conclusion summarizes the advantages and drawbacks of graphitic NDR materials and identifies future challenges.

2. FLEXIBLE ELECTRONICS

Flexible circuits require specific materials for interconnects, logic gates, power storage cells, sensing and actuation. Circuit flexibility is generally gauged by the ability to operate at tight bend radii. *Organic thin films* have lower electron mobility and optical quantum efficiency than semiconductors, however their low fabrication costs and printability have made them a good choice for large area displays, sensor arrays and bioelectronics. Current research efforts on organic materials are directed towards increasing the resistance of conjugated polymers to oxidation which is known to degrade mobility over time.[26] Increasing the resilience to bias voltage cycling and mechanical fatigue are also important research areas to improve material performance.[28,42] Shape memory is another factor which limits the electromechanical response time to between 10ms and several minutes.[23]
An alternative route pioneered by John Rogers's group at the University of Illinois[1] is to micro-machine semiconductor membranes on elastomeric substrates using the *island-bridge approach*. The islands are semiconductor devices transferred from a crystalline substrate onto a flexible substrate using lift-off techniques. Individual islands are then bridged by nanoribbons carefully engineered to obtain a flexible semiconducting mesh. Although this approach does not quite achieve the level of flexibility of organic films, it allows high performance semiconductor devices including fast transistors, multicolor light emitting diodes, temperature sensors etc. to be integrated on flexible platforms. This has opened important new possibilities for medical research for instance in optogenetics.[43]
Flexible active devices have also been made from *composite thin films*. These materials typically incorporate conductive nanoparticles (usually carbon) in an insulating elastomer.[44] This route has been very successful in making addressable arrays of conformable pressure sensors and actuators.[6,9,45,46] Generally soft conducting composites give an order of magnitude larger electromechanical coupling than silicon or GaAs, the latter's piezoresistance being 1.1% per atmosphere.[47]
Before reviewing the three classes of materials above, it is useful to examine the physical requirements that pressure sensors must meet in order to solve modern technological challenges. To our knowledge, the most stringent conditions are set by the need to image turbulent flow.[48] Currently the best pressure and shear stress sensors are micro-machined in-silico. They have dimensions of 100 microns and sensitivity of 50kPa-500kPa which is inadequate.[22] Imaging turbulence in the air boundary layer of an aircraft is an outstanding challenge[48] which calls for sensor arrays sampling pressure changes at a rate of 1kHz, with sensitivity of at least 1 kPa, and spatial resolution better than 26μm.

2.1 Organic transistors

Organic transistors are synthesized from either small conjugated molecules such as pentacene or conjugated polymers such as polythiophene or PEDOT.[26,42] The former are prepared by thermal sublimation and have been used to make addressable arrays of organic transistors with excellent flexibility.[28,45] The latter by contrast have better resistance to oxidation and higher mobility up to $0.1 cm^2 V^{-1}.s^{-1}$. Polymer films were obtained by inkjet printing,[49,50] paper-like inline printing,[51,52] subtractive lift-off lithography where the organic film is peeled off from the imprinted area,[53] spin coating,[54] thermal imprint lithography which can achieve a resolution as high as 5nm.[55,56] Beside addressable matrices of sensors, organic transistors are important for wearable electronic tags for radio-frequency identification.[51] Although the conduction mechanism is predominantly through holes, functionalization with fluorinated perylene carboxylic diimides has been used to obtain high mobility n-type conduction in organic thin films.[57]

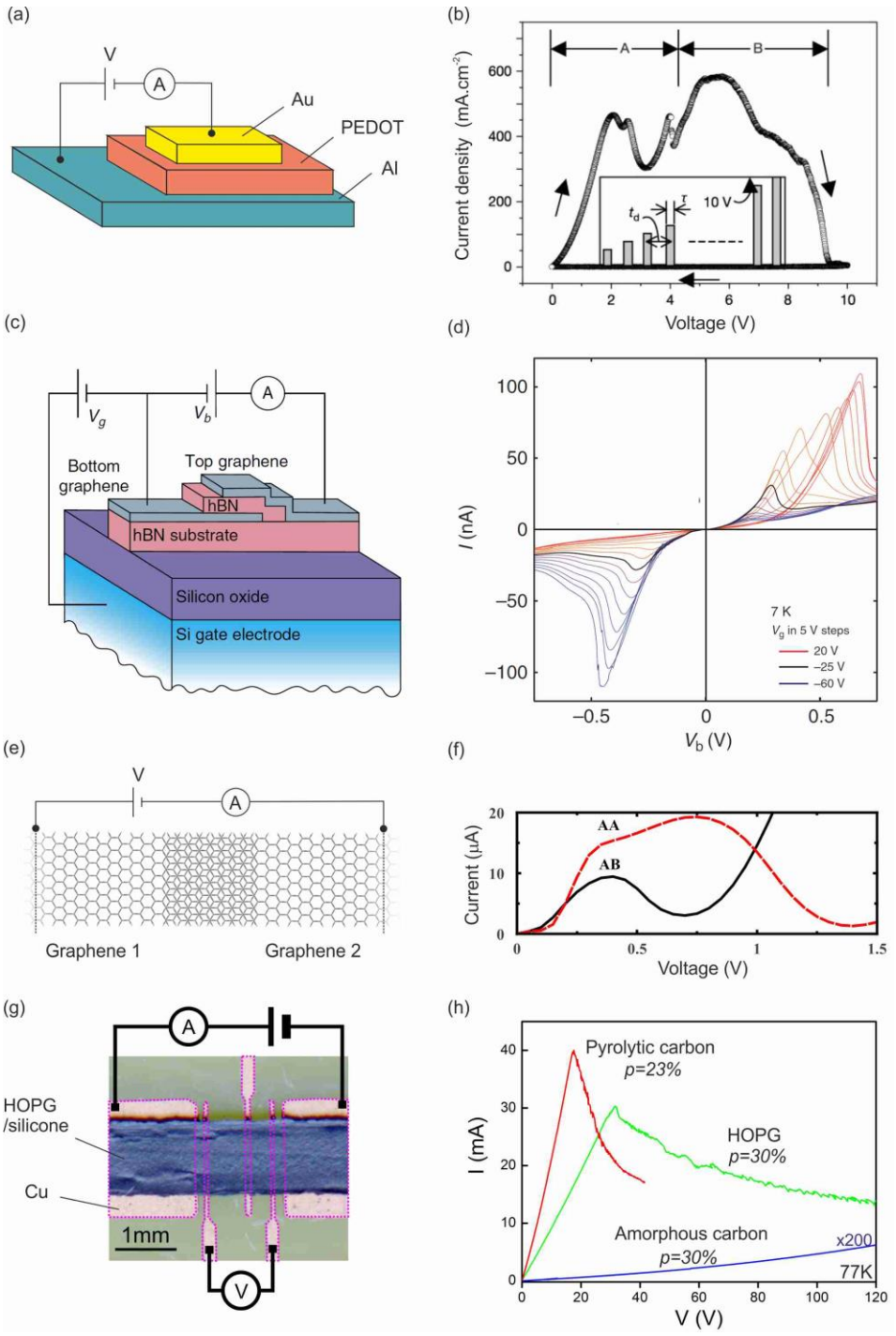

FIGURE 1 Negative differential resistance in flexible materials.
(a) PEDOT thin film (40nm) and (b) current-voltage curve with complex NDR; (c) graphene/boron-nitride/graphene trilayer and (d) current-voltage curves at different gate voltages (V_g); (e) theoretical model of electron transport across the graphene bilayer and (f) theoretical current-voltage curves ; (g) graphite-silicone composite film and (h) current-voltage curves for 3 different graphite allotropes. (Reproduced from [Möller et al. 2003] (b); [Britnell et al. 2011] (c,d); [Massum Habib et al. 2011] (e,f); [Littlejohn et al. 2011] (g,h); with permission from Nature, Wiley, Nature Communications and the American Institute of Physics.)

2.2 Composites and thin films of graphitic nanomaterials

Artificial skins have successfully been implemented that mimic the sense of touch with sensitivity approaching the detection threshold of the human skin at 0.1g/mm^2 or 1kPa.[22] This was achieved by reading the change of resistance[9,44,58] or capacitance[59,60] of soft conducting composites mixing conducting graphitic nanoparticles (carbon black, graphene, carbon nanotubes) in an elastomeric matrix: poly(propylene), poly(styrene), poly(methylmetacrylate) and poly(dimethylsiloxane) being among the most common. Such composites exhibit piezoresistance larger than 10%/atm. Transport is percolative. The conductivity depends exponentially on the hopping distance between conducting islands[61] and increases as power law of the nanoparticle filling fraction.[39,44] Composites incorporating carbon black (amorphous) nanoparticles have been used to make large area pressure sensor matrices[45], temperature sensing elements[9] on substrates such as cellulose acetate or poly(ethylene naphthalate) that allow arrays to conform to curved surfaces. Large piezoresistance with negligible shape memory has been obtained in networks of self-aligned graphene flakes.[11,39,62-64] Composites incorporating single and multiwall carbon nanotubes in poly(ethylene) and poly(propylene) matrices have also been synthesized. These obtained good pressure[12,13,23] and strain sensing properties.[65,46] Interestingly carbon nanotubes allow a degree of directional control that has enabled strain detection through changes in capacitance.[46] Sekitani et al.[6,66] have further achieved highly conductive (100 S.m^{-1}) and stretchable (100%) interconnects by dispersing single wall carbon nanotubes in fluorinated rubber and using ionic liquids as an intermediate preparation step. Wang et al. have similarly achieved high frequency operation with flexible circuits integrating semiconducting nanotube networks as interconnects.[67] Self-anchored carbon nanotubes in microcavities[68] and graphitic ink[10] have further proved to be excellent pressure sensors. These sensors were able to detect the pressure applied by fingertips which typically amounts to 50-500 kPa, a sensitivity which can be enhanced by the use of microstructured rubber layers.[24]
The enormous surface area of graphene and carbon nanotubes also affects the mechanical strength and thermal stability of the matrix even at low filling fractions (<2%) resulting in an increased Young's modulus (+30%) and glass transition temperature (+30°C).[69] Optical and thermal actuation was obtained by embedding carbon nanotubes in hydrogel.[70] Electrical actuation was achieved by fabricating carbon nanotube composites on either side of a gelatinous electrolyte which produced bi-metallic strip-like deflection under bias.[14]

2.3 Island-bridge semiconductor lattices

Membranes of metallic and semiconductor materials are better able to sustain the strain experienced by active materials during bending.[1,8] This is because, unlike in the bulk, thin ribbons are able to distribute deformation over large scales keeping local strain below the fracture threshold.[17] This principle has guided the development of the island-bridge strategy for making flexible circuits. This technology is very attractive in that it builds on the earlier development of inorganic semiconductor devices. These devices can sit on rigid islands while being interconnected via deformable metallic ribbons. The use of lift-off techniques[8] for transferring active semiconductor devices from their native substrate to a flexible substrate allows integrating III-V semiconductors such as GaN for blue light stimulation in optogenetics,[18,43] sensors and silicon circuits on the same flexible substrate.[71] This strategy does not compromise component performance since the switching speed, optical quantum efficiency[72,73,43] and chemical stability of semiconductor devices are conserved in the flexible version. This versatile strategy has led to a wealth of new applications in bioelectronics including flexible microelectrodes,[74] interconnects,[1,6] wireless power transmission,[75,67] brain mapping,[16] catheters,[71] optogenetics,[43] epidermal electronics and body wearable sensors,[15,71] bioengineered scaffolds for synthetic tissues,[76] wound monitoring electronics,[7] conformable materials such as fibroin which dissolve in biological tissues

after a healing period[77,78] and stretchable batteries.[79] Curvilinear electronics based on silicon membrane interconnects has been shown to operate on curved surfaces,[80] articulated joints and paper-like displays.[25]
A related concept has been proposed based on the graphene-graphite system.[81] This proposal envisions graphene transistors interconnected via graphite tracks. The fabrication method relies on the spatial patterning of metal catalysts to selectively activate the growth of graphene or graphite. Arrays of graphene transistors interconnected with multi-layer graphite have been used to demonstrate this concept in chemical sensing.[81]

3. MATERIALS FOR NEGATIVE DIFFERENTIAL RESISTANCE

3.1 Tunneling in semiconductors

The importance of negative differential resistance for making active devices has been recognized early on.[32] Electronic oscillators, amplifiers, and binary memories have all been realized with Esaki diodes,[82] semiconductor superlattices[83] and resonant tunneling double barrier structures.[84] These quantum tunneling devices use the electric field induced alignment of quantum energy levels to obtain regions of decreasing current giving negative differential resistance. Resonant tunneling from one 2D system in the emitter electrode of a double barrier resonant tunneling structure to another 2D system in the quantum well has been demonstrated both with electrons[85] and holes.[86] Recently negative differential resistance between 2D electron systems has been demonstrated in a graphene/h-boron nitride/graphene trilayer.[38] Double barrier resonant tunneling structures have been integrated vertically to obtain multiple peaks in the I-V curves. These systems exhibit consecutive regions of negative differential resistance which are attractive for multi-level logic.[87] Multi-level memories made from these devices have been demonstrated by several groups.[33,88,89] The physics of semiconductor tunneling devices is now well-understood. However the sensitivity of the peak-to-valley current ratio to scattering and the blurring of quantum mechanical resonances by thermo-activated current have limited their room temperature applications. Tunneling devices nevertheless occupy technological niches such as high frequency generation and heterodyne detection in radio-astronomy.[34,35]
In semiconductor tunneling devices, the stability condition is determined by the *external circuit* through the product $|g|r$ where g is the small signal conductance of the NDR region and r is the load resistance of the external circuit.[32] When $|g|r>1$, the NDR device and its eternal circuit form a bistable system which is used in memories. In the opposite case, the system oscillates spontaneously.

3.2 Intrinsic bistability, switching and NDR-like behavior of organic thin films

Since the work of pioneering work of Gregor[90] in the 1960s, a NDR–like phenomenon has also been known to exist in thin polymer films. This NDR is relevant to flexible electronics although it is essentially a charging effect, fundamentally different from the tunneling effect giving semiconductor NDR. Thin films of conjugated polymers have typically been contacted with ITO, Au or Al electrodes. The first such work measured the I-V curves of poly(divinylbenzene) contacted with Pb electrodes.[90] A sudden jump in conductivity was found between 2V and 4V when the bias voltage was swept upwards. The conductivity then remained in the high state over a few tens of millivolts before returning to the low conductivity state, yielding the NDR region in the process. When the bias voltage was retraced from 5V back to 0V, the conductivity was found to remain in the low state throughout the sweep: in other words the conductivity peak was absent. To turn on the high conductivity state again and demonstrate

reversibility, the polymer had to be biased with the opposite polarity and the voltage increased towards negative values. Because the conductivity jumps *asymmetrically* while keeping the sweep direction of the bias voltage constant, the NDR of metal/polymer films is qualitatively different from the tunneling NDR of semiconductor multilayers whose I-V curves are always *symmetrical*. Since the NDR exists only when the bias is swept up but vanishes when it is swept down, it also becomes impossible to implement metal/polymer systems as oscillators, amplifiers and memories whose state can be controlled by an external circuit.[32] This is why one applies the term "NDR-like" to conductance peaks in metal/polymer systems.

Conductance switching has been demonstrated in a wide range of metal/polymer systems. Multilevel conductance switching has been obtained by applying voltage pulses of different amplitude in poly(2-methoxy-5-(2'-ethyl-hexyloxy)-1,4-phenylene vinylene) between ITO and Al electrodes. Switching occurs above a threshold voltage which depends on the polymer film thickness and the work function of the metal in the electrodes.[91] The conductivity ratio in the high and low states was found to be as high as 10^4 in electrostatically self-assembled Rose-Bengal molecules.[92] Polymer switches are particularly relevant to WORM memories (Write Once Read Many times) for which they provide either fuses which switch open when biased by a voltage pulse[92] or anti-fuses which become conducting.[93-99] The switching to a lower conductance state was achieved in copolymers such as poly[*N*-vinylcarbazole-*co*-EU(vinylbenzoate)(2-thenoyltrifluoroacetone)$_2$-phenanthroline] (PKEu) which has both electron donors and acceptors groups obtained through electrostatic self–assembly preparation techniques.[100]

Conductivity switching occurs prior to a NDR region in poly-aniline nanofibers,[101,98] poly(methylmethacrylate-co-9-anthracenyl methylmethacrylate),[102] 2-amino-4, 5-imidazoledicarbonitrile (AIDCN),[94] poly (ehtylenedioxythiophene) (PEDOT) films,[96,97] polystyrene,[95] polypyrrole,[103] polythiophene (PCDM).[99] Fig. 1a shows a PEDOT film sandwiched between two Al electrodes which is used to measure the I-V curves shown in Fig.1b.[96] A complex peak structure is seen below 4V (region A) which is where bistability and switching between conductivity states occurs. Region B, by contrast exhibits a stable NDR region. The change in conductivity can be programmed with voltage pulses of different magnitude and duration.[96] In general, the I-V curves of most polymers have a region of bistability at lower bias voltage followed by a small NDR region at higher bias.

At the microscopic level, the mechanism underpinning the NDR and bistability has been interpreted using various charge transfer mechanisms. One mechanism is the electric field induced charge transfer from gold nanoparticles formed during the thermal evaporation process in the vicinity of contacts to acceptor sites in the polymer.[94,95,101] The release of extra conducting electrons in the LUMO of the polymer is the most frequently cited mechanism for conductivity jump. This has been corroborated by observations of the dependence of the electrical bistability on the thickness and the type of the metal in the electrodes. The charging (reduction) / discharging (oxidation) of conjugated bonds governed by the donor–acceptor sites of the polymer has also been proposed as a mechanism for bistable switching.[100,29,96,103] Molecular conformational changes under charging may play a role.[102] Recently, metal filaments have been formed in a polymer[104] to engineer a novel switching mechanism inspired from memristive alloys and to confirm the crucial role of the metal/polymer interface in the NDR.

The NDR-like phenomena of organic thin films may viewed as more closely related to Ovshinsky's switching in amorphous semiconductor alloys[105] than to quantum tunneling in band engineered semiconductors. The recent discovery of memristance in TiO_2 alloys has shown that Ovshinsky's switching could arise through the formation of conductive paths associated with reversible structural

changes in the alloy.[106,107] Interestingly both metal/organic and amorphous semiconductor memristive technologies have been competing to make the first artificial neuronal synapses which change their conductivity based on the amount of stimulation their have received up to that point. These synapses, called Spike Timing Dependent Plastic (STDP) synapses have been proposed and demonstrated based on metal/polymer thin films[108,109] and TiO_2 memristive alloys.[110] These materials are unique in emulating synaptic behavior which is essential to enabling neural networks to learn without human supervision.

3.3 Tunneling in graphene/boron nitride/graphene multilayers

Graphene films have been grown over large areas[111] and form an interesting material for flexible electronics.[112] The concept of a graphene transistor is however difficult to implement due to the impossibility in switching off the drain-source current. This is intrinsically linked to the absence of an energy band gap at the Dirac point. Recent work by Britnell et al.[38] have instead investigated transport perpendicular to the graphene layers and demonstrated robust negative differential resistance. They built the device shown in Fig. 1c which consist of 2 graphene layers sandwiching 4 monolayers of h-boron-nitride, an insulating material which provides a tunneling barrier. Britnell et al. studied the tunneling current as a function of the bias voltage V_b between the two graphene layers and a gate voltage V_g which set the Fermi level in one graphene layer relative the Dirac point in that layer. The I-V curves (Fig.1d) show a current peak which moves to higher bias voltage when the chemical potential of the gated layer increases $V_g>0$. Britnell have interpreted the current peak as occurring under specific bias condition that allow coherent tunnelling between the layers. The translational invariance of the trilayer in the plane of the layers implies that in-plane momentum must be conserved. Conservation of in-plane momentum only occurs when the Dirac points are aligned, the chemical potential is the graphene layers being exactly $\pm eV_b/2$. The dependence of the peak position on V_g arises from misalignment between Dirac points caused by electrostatic feedback. This NDR is robust up to room temperature and presents strong potential for atomically small, flexible active devices. The tunneling mechanism does not require a quantum well structure. As a result the transit time of carriers is smaller than in conventional quantum well structures which promises frequency generation in excess of the THz.[35]

The I-V curves of the graphene bilayer junction (Fig.1e) were also investigated theoretically[113] using density functional theory and non-equilibrium Green's function approach. The I-V curves were predicted to exhibit a NDR region (Fig. 1f) induced by the opening of an energy band gap in the biased graphene bilayer. This band gap is associated with the breakdown of AA or AB stacking symmetry as demonstrated by Mc Cann et al.[114,115] which is why the modeled I-V curves depend on atomic stacking (Fig.1f). The band gap of the biased graphene bilayer has been demonstrated experimentally by angle resolved photoemission spectroscopy (ARPES) in doped bilayers[116] and in gated bilayers.[117,118] Negative differential conductance has also been predicted to occur through coherent backscattering in graphene nanoribbons at the location of contacts,[119-121] in zigzag ribbon geometries[122] and via resonances through bound states.[123] Moving from the graphene bilayer to bulk graphite increases the π-band overlap to 150meV.[124] The electric field required for breaking the π-band is 4.5×10^{11}V/m which makes NDR difficult to observe in bulk graphite unless this electric field is localized to within a few graphite planes only.

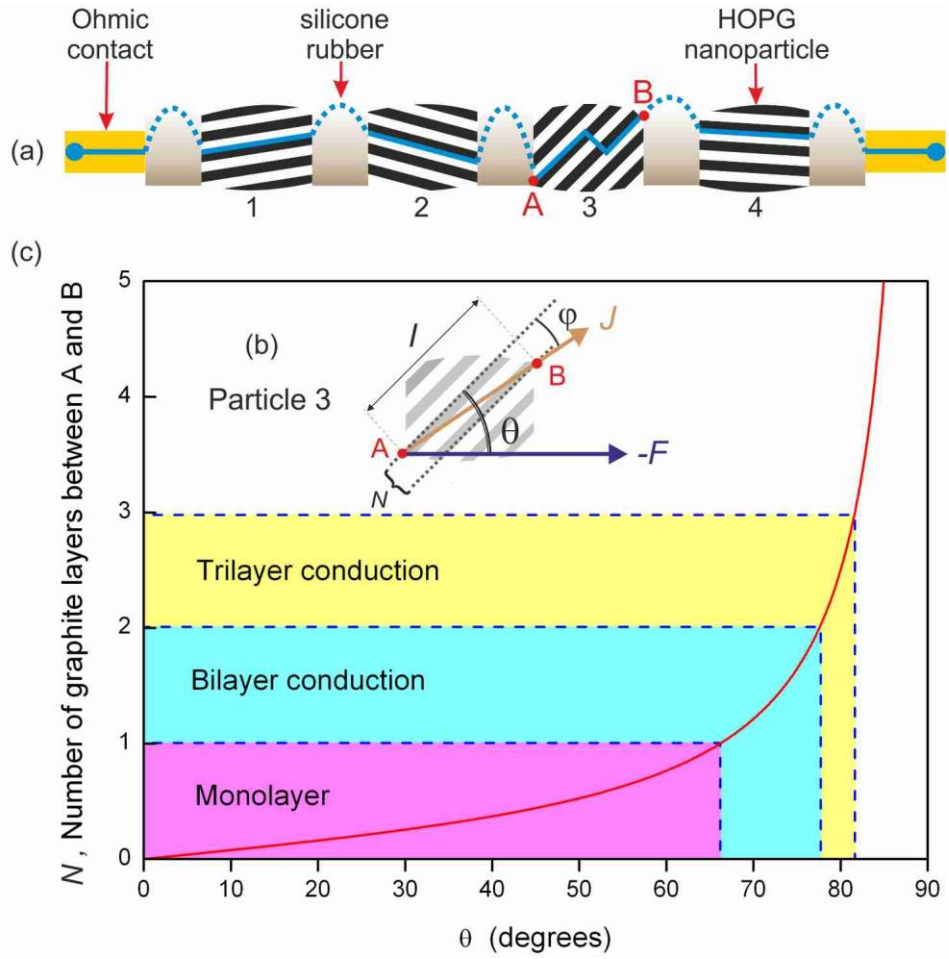

FIGURE 2 Mechanism of NDR in graphite-silicone

(a) A percolation path through randomly oriented HOPG nanoparticles (blue line). Particles 1, 2 and 4 have graphite planes tilted at a low angle ($\theta<66°$) relative to the electric field and as a result conduct through individual graphite planes. Particle 3 has a higher tilt angle ($66°<\theta<78°$) which causes the current to jump from one graphite plane to the next between the entry point A and exit point B; (b) current density and electric field inside particle 3; (c) the different conduction regimes as a function of the tilt angle θ of the graphite planes relative to the electric field.

3.4 NDR of graphite-silicone composites

Composites of graphitic nanoparticles in polymethylsiloxane (silicone) have also attracted attention for their robust NDR[37,39] which has been put to work in actual flexible devices such as electronic amplifiers and pressure sensors.[36] Silicone is flexible but insulating. In order to make the material conduct, several groups have synthesized composites by mixing in metallic or semiconductor nanoparticles. Graphitic materials such as carbon black nanoparticles,[58,44] graphene[11] and graphite[61] are particularly well suited as their density is close to that of silicone so that the mixture is effectively homogeneous. The composite effectively behaves as a percolation network in which transport is controlled by tunneling

assisted hopping from one nanoparticle to the next.[36,37] The composite conductivity was shown to exhibits a power law dependence on the nanoparticle filling fraction which is characteristic of percolation.[36,37] Graphite-silicone composites are prepared by mixing graphitic nanoparticles in liquid silicone using pestle and mortar until the mixture is homogeneous. A stannane based catalyst is then dissolved prior to molding the composite. Littlejohn et al. have used Hall bar shaped molds[36] for their active devices (Fig.1g). Composite Hall bars with 50μm wide channels have been obtained by micro-machining molds in a silicon substrate using optical lithography and reactive ion etching. After filling the hollow Hall bar with composite, the surface of the wafer was coated with a layer of pristine silicone. This layer provides a flexible insulating substrate for the composite devices to stand on once the assembly is removed from to mold. The assembly is left to cure at room temperature for 24h prior to unmolding. This approach has obtained micron sized electronically active devices on substrate with identical mechanical properties and excellent chemical stability.

Low temperature transport has been studied by Littlejohn et al. who measured I-V curves of graphite-silicone thin films between 4K and 300K.[36,37,39] At 77K, the I-V curves of composites filled with Highly Oriented Pyrolytic Graphite nanoparticles (450nm) exhibit a current peak followed by a NDR region (Fig.1h). The I-V curves are completely symmetrical with respect to a change in bias polarity. The NDR region is independent of the direction in which the bias voltage is swept. The I-V curves show a small dependence on the rate of bias sweep, the current peak becoming more rounded when the sweep rate increases.[39] The current, which increases smoothly before the peak, decreases by jumps in the NDR region. These small current jumps are not always reproducible and may be related to the stochastic nature of percolation. Despite these jumps, the current was found to decrease monotonically up to the breakdown voltage (Fig.1h).[39] The peak-to-valley current ratio was 2.5:1 at break down (77K) which marked the upper limit of the NDR region. This underlines a key difference with semiconductor tunneling devices whose NDR region has finite width. The composite NDR depends strongly on the crystalline structure of the filler nanoparticles. Littlejohn et al. studied composites filled with 3 different carbon allotropes. The I-V curves in Fig.1h reveal that sp_2 bonding - associated with the formation of graphite planes - is essential to the formation of a NDR region. HOPG and pyrolytic graphite nanoparticles give NDR but not amorphous carbon. Another characteristic of the composite NDR is that it disappears when the I-V curves are measured on scales smaller than ~0.1mm at volume filling fraction of 32%.[36] The peak current was associated with the formation of electric field domains in the composite film.[125] The position of the current peak can be tuned with the HOPG filling fraction. The current peak moves to lower bias with increasing HOPG content.

When the temperature increases from 77K upwards, the peak position decreases towards zero bias voltage and vanishes at 210K[39]. Between 210K and 300K, the I-V curves increase monotonically. A small sub-linear trend is observed which is consistent with thermal expansion of the silicone matrix under Joule heating.[126,127,61] The low temperature current peak is an altogether distinct phenomenon. Measurements of in-situ temperature show that Joule heating raises the film temperature by a few degrees at the peak while silicone remains below its glass transition temperature. Further, the composite can oscillate at frequencies faster that 10kHz in the NDR region which is faster than the thermal relaxation rate. These observations suggest that the low temperature NDR originates in the percolation transport through HOPG nodes of anisotropic conductivity.

Above the percolation threshold, percolation paths behave as depicted in Fig.2a. The nodes of the percolation network are HOPG nanoparticles with random orientations θ relative to the electric field

applied by the contacts. Conduction in graphite is known to be highly anisotropic being 3000 times larger along the graphite planes than in the perpendicular direction.[124] The current entering a 450nm wide HOPG nanoparticle will be carried by the same graphite plane as long as $\theta<66°$ (Fig.2b). It will enter one graphite plane and exit the next neighboring plane when $66°<\theta<78°$. It will cross more graphitic planes when $\theta>78°$ approaching 90°. The number of layers crossed as a function of tilt angle is plotted in Fig.2c. The majority of HOPG nanoparticles (labeled 1,2 and 4 in Fig.2a) will thus give low resistance associated with in-plane conduction. A relatively small number of nanoparticles for which $\theta>78°$ will be too resistive to belong to any percolation path. Nanoparticles with intermediate tilt angle, such as particle 3 in Fig.2a support bilayer conduction. These particles conduct at low electric field bellow the critical value ($4.5x10^{11}$V/m) which breaks the π-band overlap in graphite (150meV).[124] Above this critical electric field, nanoparticle 3 undergoes a semimetal to insulator transition.[39,113-117] A theory of tunneling through a single silicon barrier between two HOPG electrodes was built.[39] This theory predicts an infinitely wide NDR region as the electric field increases beyond the critical value which causes type 3 HOPG nanoparticles to become insulating. Littlejohn et al. calculated the theoretical I-V curves and predicted the correct dependence on temperature and HOPG filling fraction.[39]

Nanoparticles undergoing metal-insulator transition (type 3) are believed to form the boundaries of the electric fields domains. A metal-insulator transition can only occur in sp_2 hybridized nanoparticles which explains why the NDR is only observed in HOPG and pyrolytic graphite nanoparticles. The tunneling theory[39] was also used to fit the dependence of the peak position on temperature between 77K and 200K. Temperature increases the thermoactivated current making the silicone barrier increasing conductive as temperature increases. As a result a larger fraction of the total applied bias is supported by graphite nanoparticles. The increase of the electric field across nanoparticles of type 3 causes the metal-insulator transition to be reached at lower bias when temperature increases. A fit of the thermal activation plot gives a tunneling barrier height of 165meV in the HOPG/silicone/HOPG system.[39]

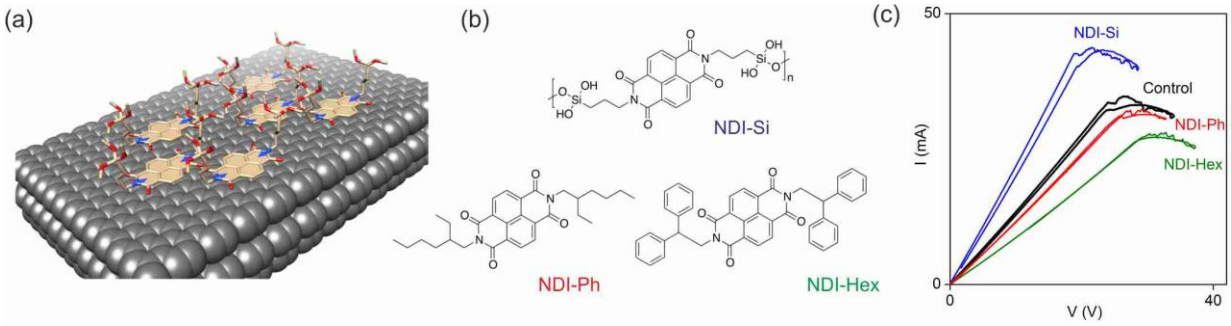

FIGURE 3 Functionalization of the HOPG-silicone interface with naphthalene-diimide (NDI)
(a) The benzene cores of NDI molecules adhere to graphite nanoparticles via Van der Waals interactions whilst the appendages bind to silicone chains in the matrix; (b) the three types of NDI molecules used as functionalization agents are NDI-Si ($C_{26}H_{34}N_2O_{10}Si_2$), NDI-Hex ($C_{30}H_{38}N_2O_4$), NDI-Ph ($C_{42}H_{30}N_2O_4$); (c) the current-voltage curves of the functionalized composites and the control sample. Measurements were taken at 77K.
(Reproduced from [Littlejohn et al. 2011] (a,b); with permission from Wiley).

Tunneling theory predicts that the NDR would be observed above room temperature if the tunneling barrier height could be increased to at least 250meV.[39] To this end, Littlejohn et al. have sought to tune the tunneling barrier by functionalizing the graphite/silicone interface with supramolecular assemblies (Fig.3a). Several groups have used perylenedicarboximide (PDI) templates in surface chemistry to modify the local electronic properties of graphene.[128-131] This has the effect of opening an energy band gap at the Dirac point.[132,133] Organic transistors have further been obtained based on PDI derivatives.[57] An enhancement of the optical quantum efficiency has been achieved by adsorbing pyrene and perylene diimide on the graphene surface.[62] Graphene sheets functionalized with poly(acrylonitrile) and poly(methylmethacrylate) have shown improvement in glass transition temperature, mechanical strength and thermal stability.[69] Recently naphthalediimide molecules have also been used.[134,135] These molecules have the benzene ring core structure shown in Fig.3b but offer more versatility than PDI in attaching various appendages. Littlejohn et al. have used molecules synthesized with three different appendages (Fig.3b) to tune the I-V curves and the NDR region (Fig.3c).[39] The core of the molecule attaches to the surface of HOPG nanparticles via van der Waals interactions. NDI-Si appendages bond covalently to the –[Si-O]- polymeric chains of the matrix giving the composite with the lowest resistance in Fig.3c. The other appendages (NDI-Ph, NDI-Hex) have high steric volume and a chemical structure mismatched to that of the matrix. Unsurprisingly, NDI-Ph and NDI-Hex functionalization increases the resistance of the composite. Fig.3c thus shows that the physical characteristics of the silicone barrier can be tuned using chemical functionalization of the graphite surface.

4. ELECTROMECHANICAL RESPONSE OF STRAINED NDR DEVICES

Littlejohn and et al.[36] have incorporated graphite-silicone composites in a LC circuit resonator to make the composite oscillate spontaneously in order to demonstrate its ability to function as an electronically active material. Littlejohn et al. biased thin composite films in the NDR region with a load line of slope $1/r$ (0.5mS) steeper than the negative differential conductance $|g|$ (~1mS) so that the system exhibits a single - unstable - operating point in the NDR region. The time series oscillations of the composite are shown in Fig.4a. Their frequency dependence obey the law $2\pi f_{LC} = \sqrt{1/LC - g^2/C^2}$ where L and C are the inductance and capacitance of the resonant circuit (Fig.4b). The frequency of spontaneous oscillations was verified to decrease when the capacitance C is reduced (Figs.4c,d).

The spontaneous oscillations of composites are more complex than those generated by semiconductor multilayers. This can be seen in Fig.1a which shows multi-mode frequency generation. Spectral analysis of these oscillations[36] reveals *a natural mode of oscillations* besides the *driven oscillation mode* set by the LC circuit. By varying L and C it is possible to make the composite oscillate over a 0-25kHz bandwidth. The upper limit of this range corresponds to the intrinsic cut-off capacitance of the composite which depends on the HOPG filling fraction. In contrast to the driven mode, the natural mode is self-oscillations of the composite which occur in the NDR region without any external circuit. This mode is independent of L or C and is observed even after these components have been removed. The natural mode usually oscillates at a frequency higher than the cut-off frequency of the driven mode. The same bimodal frequency generation has been observed in several composites. The frequency of the natural mode increases with increasing pressure and graphite filling fraction. The natural mode is ascribed to drip-like percolation through the composite.[36]

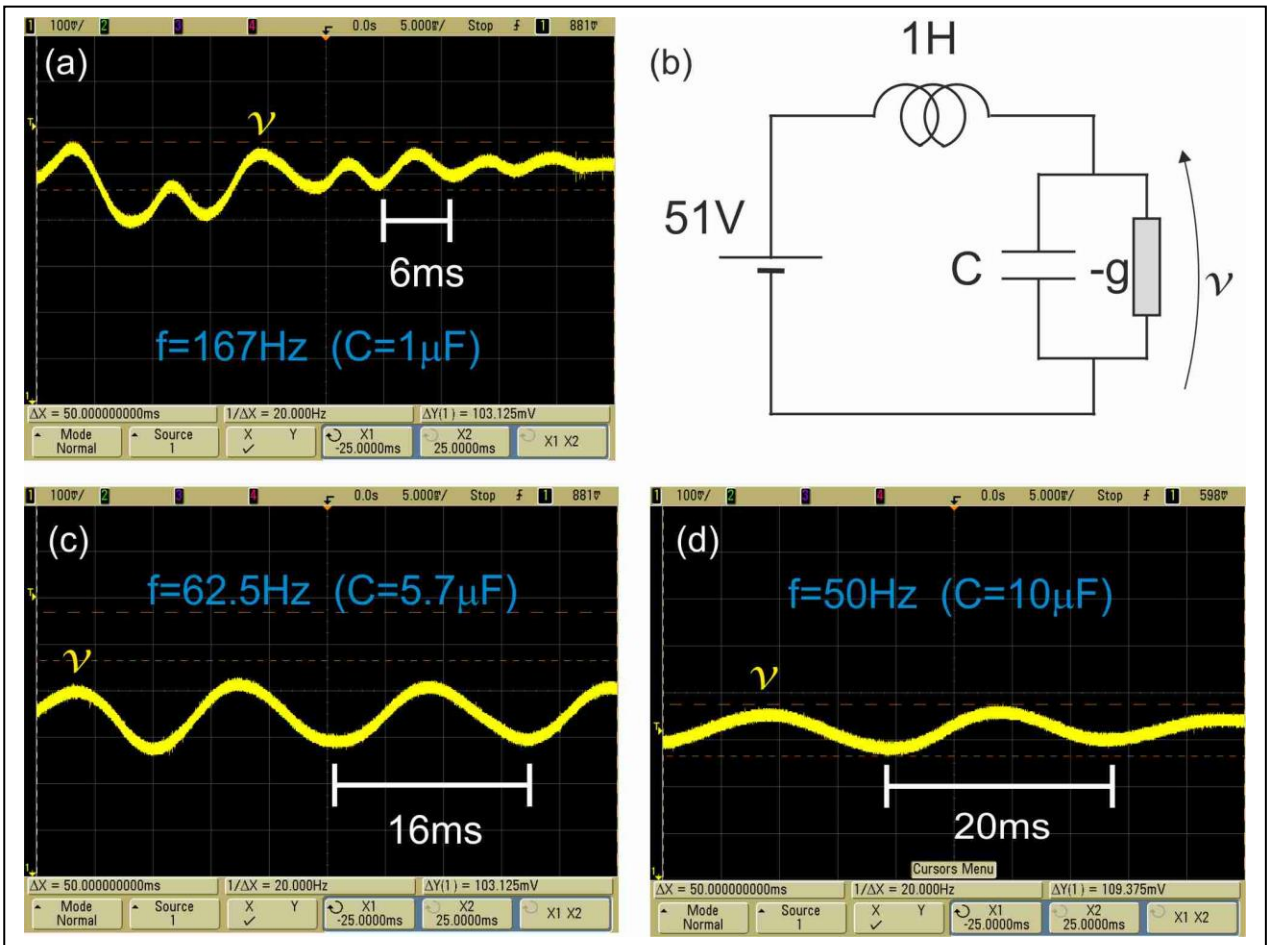

FIGURE 4 Electrical oscillations of graphite-silicone composites in the NDR region.
(a) Oscilloscope screenshot of composite oscillations at frequency f_{LC}=167Hz; (b) LC resonator circuit, the composite is represented by its negative differential conductance -*g*; (c) f_{LC}=62.5Hz; (d) f_{LC}=50Hz.

Having demonstrated the active properties of the material, the next step is to investigate electrical behavior when the material is deformed. To this end, Littlejohn et al.[36] have synthesized graphite-silicone thin Hall bars on stretchable and bendable substrates which are shown in Figs.5a,b and Fig.5c respectively. The Hall bar in Fig.5a was prepared by imprint lithography and overlaid on pristine silicone substrate. Silicone substrates allow stretchable devices. The imprint mask consisted Hall bars molds prepared by optical lithography and plasma etched to a depth of 200μm. The mask was coated with silicone oil to facilitate extrusion. The graphite silicone composite was then applied to fill the groovy pattern using a plastic blade. A uniform film of pristine silicone was then compression molded at the surface of the imprint mask to form a flexible substrate for the composite Hall bars. The pristine silicone/composite bilayer was allowed to set for 24 h to form rubber, after which the silicone bilayer was peeled giving the devices shown in Fig.5a,b. Through this technique it is possible to fabricate silicone/silicone composite circuits of very small dimensions. The Hall bars prepared by Littlejohn et al.[36] had channel widths down to 50μm. The other types of composite devices are shown in Fig.5c.

These were molded on cellulose acetate sheets using similar methods. Cellulose acetate substrates bend but do not stretch given that their Young's modulus (E≈400MPa) is much larger than that of silicone (E≈4MPa). The composite/acetate bilayer was then bent to apply controlled interfacial strain ε (Fig.5c). The bilayer strain was calculated from the relative change in the chord $\eta = (l_0 - l)/l_0$ using Timoschenko's formula.[136] The interfacial stress at 300K was calculated form Stoney's formula.[137]

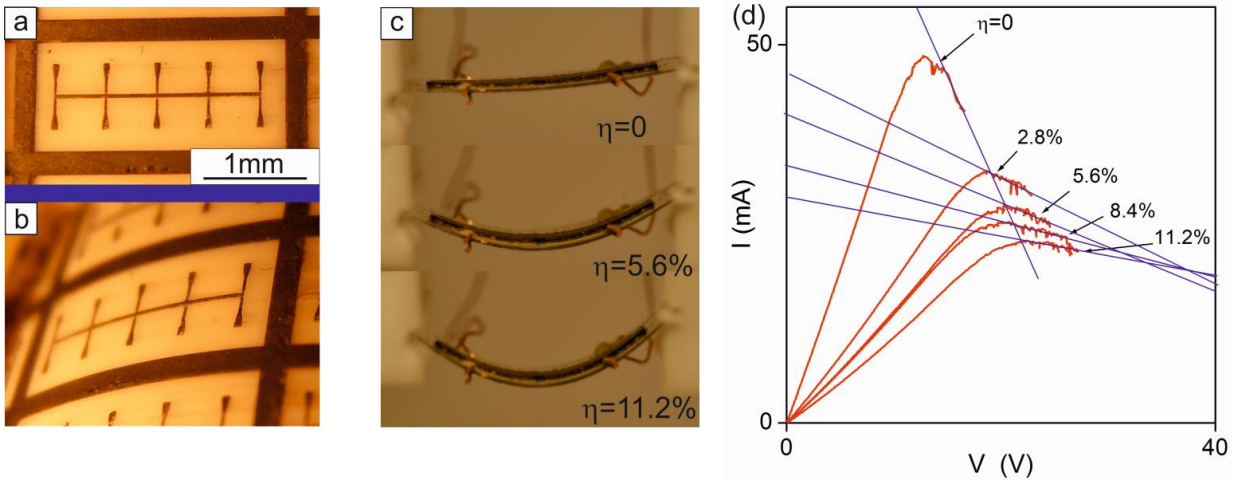

FIGURE 5 Dependence on the NDR on the curvature of a graphite-silicone film
(a) Graphite silicone hall bar fabricated on a pristine silicone substrate ; (b) same device when bent; (c) applying compressive strain (η) by bending a composite/acetate bilayer ; (d) I-V curves of the composite film under increasing strain.

Increasing the strain has the effect of lowering the composite resistance and *decreasing the negative differential conductance g* - see Fig.5c. The reduction of *g* is observed whether the composite film is put in tension or compression. This attribute of the electromechanical response has also been reported in silicon membranes.[1,138] The peak position moves to higher bias voltage with increasing strain. However as long as the composite remains biased in the NDR region, the composite continue to oscillate. In fact, strain makes these oscillations easier to observed because the condition |g|r<1 is relaxed. The low temperature experiments require the composite to be cooled down at 77K and then warmed up to room temperature for the curvature of the film to be increased. The I-V curves were measured again after decreasing the curvature of the composite from bent to flat. The data in Ref.36 show that the composite is remarkably resilient to temperature and mechanical cycling. Although the low temperature strain is very similar to the one applied at room temperature, low temperature stress is unknown in particular as silicone crosses its glass transition temperature at 230°C each time.

Littlejohn et al. have next investigated the effect of strain on the spontaneous oscillations shown in Fig.4. The results are plotted as maps of the power spectral density as a function of the resonant frequency of the LC cavity for 3 different values of the applied strain (Figs.6a-c). Figs.6b&c clearly shows the bimodal spectrum of spontaneous oscillations: the *cavity mode* increases linearly with f_{LC}, while the *natural oscillation mode* (labelled B) has no dependency dependence on f_{LC}. Strain affects the both oscillation

modes via the reduction in negative differential conductance, *g,* as seen in Fig.5d. Firstly, strain increases the cut-off frequency of *the cavity mode.* The cut-off frequency is given by:[32] $2\pi f_r = g/C_r\sqrt{1/gr-1}$ where $C_r = gL/r$. Therefore, if $gr << 1$, the cut-off frequency is $f_r \propto g^{-1/2}$ and since *g* decreases with strain, f_r will increase will increasing strain. Secondly strain also increases the frequency of the *natural mode*, see line B in Figs.6a-c. In this mode, the composite behaves as a strain sensor that encodes strain into frequency. The empirical frequency-strain relationship is plotted in Fig.6d and is approximately linear with a slope of $\lambda = 84$ Hz/% strain. It is interesting to compare the frequency response of the composite with the change in frequency of mechanoreceptor neurons in the skin (Merkel cells).[40,41] Fig.6e shows the voltage oscillations induced in one such receptor during the time interval in which pressure is applied to the skin.[40] The frequency response to an increasing force (Fig.6f) is qualitatively the same as that of the composite in Fig.6d. This effect opens up the possibility that flexible NDR might be used to make artificial skins.

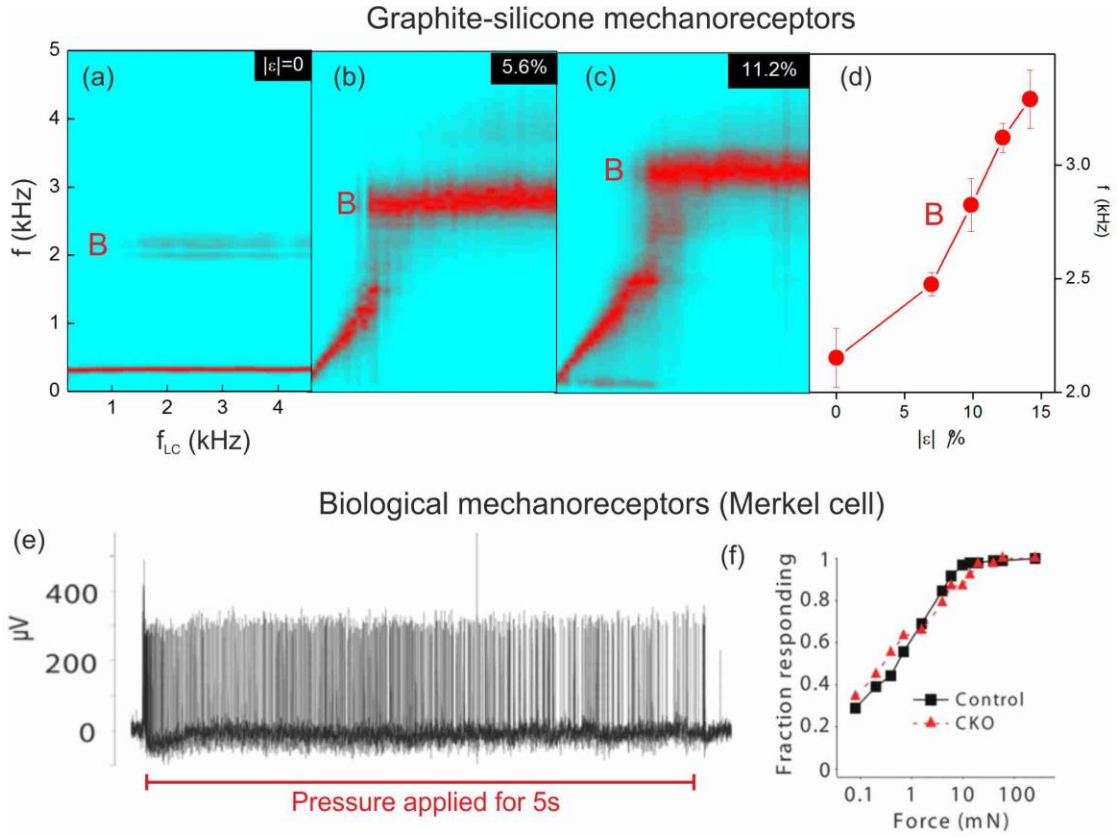

FIGURE 6 Mechanoreceptors that encode strain into the frequency of electrical oscillations
(a-c) maps of the power spectral density output by the oscillator of Fig.4 as a function for the resonator frequency f_{LC}, the bilayer strain increases from 0 to 11.2% causing the frequency of natural oscillations (Line B) to increase; (d) frequency of natural oscillations (line B) plotted as a function of strain (ε); (e) Voltage oscillations generated by mechanoreceptors in the skin when subjected to pressure over a time interval of 5s; (f) threshold/frequency dependence of voltage oscillations with strain.
(Reproduced from [Maricich et al. 2009] (e,f) with permission from the American Association for the Advancement of Science).

5. APPLICATIONS OF FLEXIBLE NDR

The observation of NDR in flexible composites is paving the way towards other classes of active devices. Littlejohn et al.[36] have demonstrated *voltage amplification* by using the composite as the active element (-*g*) of the tuned amplified circuit of Fig.7a. The circuit is able to amplify a 1kHz signal with a gain determined by $A_V = 1/(1-gr)$. The amplitude of the amplified signal in Fig.7b fluctuates over time due to nonlinearities in the material. However the voltage gain varies according to the theoretical curve of the tuned amplifier when the series resistance *r* is varied.

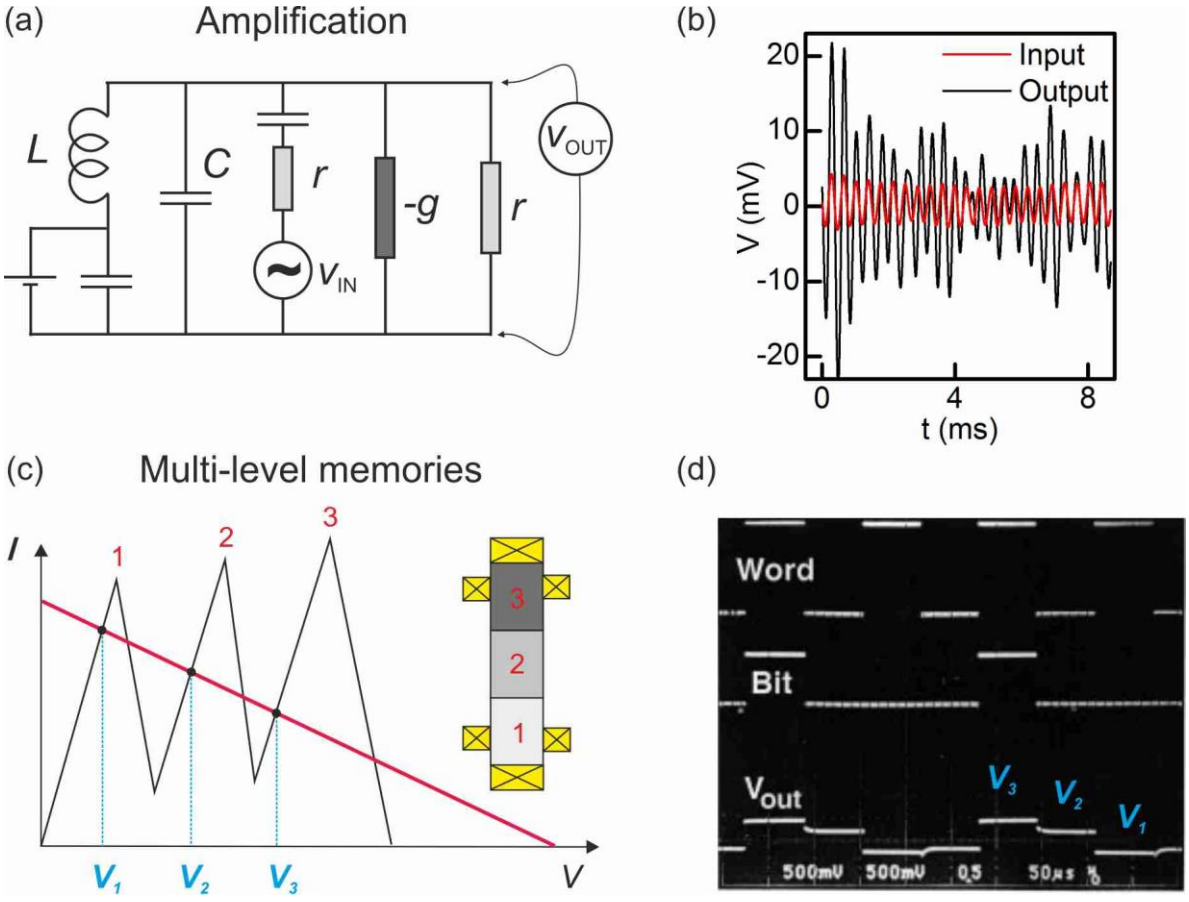

FIGURE 7 A tuned NDR amplifier made from graphite-silicone and multi-level memories
(a) Tuned NDR amplifier circuit incorporating the composite element through the negative differential conductance –g; (b) the input signal and amplified output signal generated by the NDR amplifier; (c) principle of operation of a three level memory consisting of three composite sections of decreasing HOPG filling fraction (regions 1→3 in the inset) which are connected in series; (d) three level logic. (Reproduced from [Van der Wagt et al. 1998] (d) with permission from IEEE Elect Dev. Lett.).

Multilevel logic memories are another type of application for flexible NDR. These devices require the NDR material to be biased in the bistable regime, $|g|r>1$, so that the load line of the external circuit intersects the I-V curve at more than one point. To obtain multiple stable levels, Capasso et al.[33] and other groups[87-89] have vertically integrated several double barrier resonant tunneling structures which give multiple peaks in the I-V curves. A single load line intercepting these peaks obtains multiple stable states over a range of bias voltage (Fig.7c). Van der Wagt et al.,[89] Wei et al.[88] and Capasso et al.[33] have demonstrated multiple level memory devices based on this principle. I-V curves with multiple peaks may also be obtained with composite materials. By integrating sections of composite film with graded HOPG filling fraction in series, as pictured in the inset to Fig.7c, the peak current will be obtained at different values of the total applied voltage. The section with the lowest HOPG filling fraction will initially support the largest electric field and give the first current peak. The next current peak will occur in the section with the next higher HOPG filling fraction and so on. This concept may be used to design flexible multilevel memories.

CONCLUSION AND FUTURE DIRECTIONS

Perpendicular transport through graphene and h-boron nitride multilayers offers a novel route towards NDR based active electronics. The materials are cheap, flexible, atomically thin and give NDR with higher peak-to-valley current ratio than earlier semiconductor multilayers. They have demonstrated active devices in the form of pressure sensors and amplifiers.

Future challenges include:

- Engineering tunneling barriers to quench the thermo-activated current and maximize the peak-to-valley ratio at room temperature. A promising route is by functionalizing the graphene surface with NDI or PDI molecules or by growing defect free h-boron nitride/graphene junctions.
- Limiting the effects of Joule heating and associated non-linearities.
- Widening the bandwidth of composite oscillators.
- Studying the metal-insulator transition at the scale of individual HOPG nanoparticles.

ACKNOWLEDGEMENTS The author wishes to thank DSTL(UK) who has partially supported this work under grants CDE28143 and CDE32154.

REFERENCES:

1. Khang, D.-Y.; Jiang, H.; Huang, Y.; Rogers, J. A. A stretchable form of single-crystal silicon for high-performance electronics on rubber substrates, *Science* **2006**, *311*, 208-212.
2. Park, S.-I.; Le, A.-P.; Wu, J.; Huang, Y.; Li, X.; Rogers, J. A. Light emission characteristics and mechanics of foldable inorganic light-emitting diodes, *Adv. Mat.* **2010**, *22*, 3062-3066.
3. Burroughes, J. H.; Bradley, D. D. C.; Brown, A. R.; Marks, R. N.; Mackay, K.; Friend, R. H.; Burns, P. L.; Holmes, A. B. Light-emitting diodes based on conjugated polymers, *Nature*, **1990**, *347*, 539-541.
4. Stirringhaus, H.; Tessler, N.; Friend, R. H. Integrated optoelectronic devices based on conjugated polymers, *Science* **1998**, *280*, 1741-1744.
5. Park, S.-I.; Xiong, Y.; Kim, R.-H.; Elvikis, P.; Meitl, M.; Kim, D.-H.; Wu, J.; Yoon, J.; Yu, C.-J.; Liu, Z.; Huang, Y.; Hwang, K.-C.; Ferreira, P.; Li, X.; Choquette, K.; Rogers, J. A. Printed assemblies of

inorganic light-emitting diodes for deformable and semitransparent displays, *Science* **2009**, *325*, 977-981.

6. Sekitani, T.; Noguchi, Y.; Hata, K.; Fukushima, T.; Aida, T.; Someya, T. A rubberlike stretchable active matrix using elastic conductors, *Science* **2008**, *321*, 1468-1472.
7. Kim, D.-H.; Wang, S.; Keum, H.; Ghaffari, R.; Kim, Y.-S.; Tao, H.; Panilaitis, B.; Li, M.; Kang, Z.; Omenetto, F.; Huang, Y.; Rogers, J.A. Thin, flexible sensors and actuators as "instrumented" surgical sutures for targeted wound monitoring and therapy, *Small* **2012**, *8*, 3263-3268.
8. Kim, D.-H.; Ahn, J.-H.; Choi, W. M.; Kim, H.-S.; Kim, T.-H.; Song, J.; Huang, Y. Y.; Liu, Z.; Lu, C.; Rogers, J. A. Stretchable and foldable silicon integrated circuits *Science* **2008**, *320*, 507-511.
9. Someya, T.; Kato, Y.; Sekitani, T.; Iba, S.; Noguchi, Y.; Murase, Y.; Kawaguchi, H.; Sajurai, T. Conformable, flexible, large-area networks of pressure and thermal sensors with organic transistor active matrixes, *Proc. Nat. Acad. Sci.* **2005**, *102*, 12321-12325.
10. Webb, A. J.; Szablewski, M.; Bloor, D.; Atkinson, D.; Graham, A.; Laughlin, P.; Lussey, D. A multi-component nanocomposite screen-printed ink with non-linear touch sensitive electrical conductivity, *Nanotechnology* **2013**, *24*, 165501.
11. Chen, L.; Chen, G.; Lu, L. Piezoresistive study of finger-sensing silicone rubber/graphite nanosheet composites, *Adv. Func. Mat.* **2007**, *17*, 898-904.
12. Ishigure, Y.; Iijima, S.; Ito, H.; Ota, T.; Unuma, H.; Takahashi, M.; Hikichi, Y.; Suzuki, H. Electrical and elastic properties of conductor-polymer composites, *J. Mat. Sci.* **1999**, *34*, 2979-2985.
13. Takahashi, T.; Takei, K.; Gillies, A. G.; Fearing, R. S.; Javey, A. Carbon nanotube active-matrix backplanes for conformal electronics and sensors, *Nanoletters* **2011**, *11*, 5408-5413.
14. Fukuda, K.; Sekitani, T.; Zschieschang, U.; Klauk, H.; Kuribara, K.; Yokota, T.; Sugino, T.; Asaka, K.; Ikeda, M.; Kuwabara, H.; Yamamoto, T.; Takimiya, K.; Fukushima, T.; Aida, T.; Takamiya, M.; Sakurai, T.; Someya, T. A 4V operation, flexible Braille display using organic transistors, carbon nanotubes actuators and organic static random-access memory, *Adv. Func. Mat.* **2011**, *21*, 4019-4027.
15. Kim, D.-H.; Lu, N.; Ma, R.; Kim, Y.-S., Kim, R.-H.; wang, S.; Wu, J.; Won, S. M.; Tao, H.; Islam, A.; Yu, K. J.; Kim, T.-I.; Chowdhury, R.; Ying, M.; Xu, L.; Li, M.; Chung, H.-J.; Keum, H.; McCormick, M.; Liu, P.; Zhang, Y.-W.; Omenetto, F. G.; Huang, Y.; Coleman, T.; Rogers, J. A. Epidermal electronics, *Science* **2011**, *333*, 838-843.
16. Viventi, J.; Kim, D.-H.; Vigeland, L.; Frechette, E. S.; Blanco, J. A.; Kim, Y.-S.; Avrin, A. E.; Tiruvadi, W. R.; Hwang, S.-W.; Vanleer, A. C.; Wulsin, D. F.; Davis, K.; Gelber, C. E.; Palmer, L.; van der Spiegel, J.; Wu, J.; Xiao, J.; Huang, Y.; Contreras, D.; Rogers, J. A.; Litt, B. Flexible, foldable actively multiplexed, high-density electrode array for mapping brain activity *in-vivo*, *Nature NeuroSci*. **2011**, *14*, 1599-1607.
17. Rogers, J. A.; Lagally, M. G.; Nuzzo, R. G. Synthesis, assembly and applications of semiconductor nanomembranes, *Nature* **2011**, *477*, 45-53.
18. Kim, T.-I.; Jung, Y. H.; Song, J.; Kim, D.; Li, Y.; Kim, H.-S.; Song, I.-S.; Wierer, J. J.; Pao, H. A.; Huang, Y.; Rogers, J. A. High-efficiency. Microscale GaN light-emitting diodes and their thermal properties on unusual substrates, *Small* **2012**, *11*, 1643-1649.
19. Ying, M.; Bonifas, A. P.; Lu, N.; Su, Y.; Li, R.; Cheng, H.; Ameen, A.; Huang, Y.; Rogers, J. A. Silicon nanomembranes for fingertip electronics, *Nanotechnology* **2012**, *23*, 344004.

20. Humayun, M. S.; Weiland, J. D.; Fujii, G. Y.; Greenberg, R.; Williamson, R.; Little, J.; Mech, B.; Cimmarusti, V.; van Boemel, G.; Dagnelie, G.; de Juan Jr, E. Visual perception in a blind subject with a chronic microelectronic retinal prosthesis, *Vision research* **2003**, *43*, 2573-2581.
21. Fitzsimmons, N. A.; Drake, W.; Hanson, T. L.; Lebedev, M. A.; Nicoledis, M. A. L. Primate reaching cued by multichannel spatiotemporal cortical stimulation, *J. NeuroSci* **2007**, *27*, 5593-5602.
22. Boland, J. J.; Flexible electronics: within touch of artificial skin, *Nature Mat.* **2010**, *9*, 790-792.
23. Takei, K.; Takahashi, T.; Ho, J. C.; Ko, H.; Gillies, A. G.; Leu, P. W.; Fearing, R. S.; Javey, A. Nanowire active-matrix circuitry for low-voltage macroscale artificial skin, *Nature Mat.* **2010**, *9*, 821-826.
24. Mannsfeld, S. C. B.; Tee, B. C. –K.; Stoltenberg, R. M.; Chen, C. V. H. –H.; Barmann, S.; Muir, B. V. O.; Sokolov, A. N.; Reese, C.; Bao, Z. Highly sensitive flexible pressure sensors with microstructured rubber dielectric layers, *Nature Mat*. **2010**, *9*, 859-864.
25. Gelinck, G. H.; Huitema, H. E. A.; Van Veenendaal, E.; Cantatore, E.; Schrijnemakers, L.; Van der Putten, J. B. P. H.; Geuns, T. C. T.; Beenhakkers, M.; Giesbers, J. B.; Huisman, B.-H.; Meijer E. J.; Benito, E. M.; Touwslager, F. J.; Marsman, A. W.; Rens, J. E.; De Leeuw, D. M. Flexible active-matrix displays and shift registers based on solution-processed organic transistors, *Nature Mat.* **2004**, *3*, 106-110.
26. Klauk, H. Organic thin film transistors, *Chem. Soc. Rev.* **2010**, *39*, 2643-2666.
27. Klauk, H.; Zschieschang, U.; Pflaum, J.; Halik, M. Ultralow-power organic complementary circuits, *Nature*, **2007**, *445*, 745-748.
28. Sekitani, T.; Zschieschang, U.; Klauk, H.; Someya, T. Flexible organic transistors and circuits with extreme bending stability, *Nature Mat*. **2010**, *9*, 1015-1022.
29. Tao, N. J. Electron transport in molecular junctions, *Nature Nanotech*. **2006**, *1*, 173.
30. Köhler, A.; Wilson, J. S.; Friend, R. H. Fluorescence and phosphorescence in organic materials, *Adv. Mat.* **2002**, *14*, 701-707.
31. Müllen, K; Scherf, U. Organic light emitting devices, Willey **2006**.
32. Chow, W. F. Principles of tunnel diode circuits, Wiley: New York, **1964**.
33. Capasso, F.; Sen, S.; Beltram, F.; Lunardi, L. M.; Vengurlekar, A. S.; Smith, P. R.; Shah, N. J.; Malik, R. J.; Cho, A. Y. Quantum functional devices: Resonant-tunneling transistors, circuits with reduced complexity and multiple valued logic, *IEEE Trans. Elect. Dev.* **1989**, *36*, 2065-2082.
34. Luryi, S.; Frequency limit of double-barrier resonant-tunneling oscillators, *Appl. Phys, Lett.* **1985**, *47*, 490-492.
35. Brown E. R.; Soderström, J. R.; Parker, C. D.; Mahoney, L. J.; Molvar, K. M.; McGill, T. C. Oscillations up to 712 GHz in InAs/AlSb resonant-tunneling diodes, *Appl. Phys. Lett.* **1991**, *58*, 2291-2293.
36. Littlejohn, S.; Nogaret, A.; Prentice, G. M.; Pantoş, G. D. *Adv. Func. Mat.* **2013**, DOI 10.1002/adfm.201300519
37. Littlejohn S.D. Electrical properties of graphite nanoparticles in silicone: Flexible oscillators and electromechanical sensing (Springer Theses); Eds; Springer: **2013**. ISBN-13 978-3319007403
38. Britnell, L.; Gorbachev, R. V.; Geim, A. K.; Ponomarenko, L. A.; Mishchenko, A.; Greenaway, M. T.; Fromhold, T. M.; Novoselov, K. S.; Eaves, L. Resonant tunneling and negative differential conductance in graphene transistors, Nature Comm. **2013**, DOI: 10.1038/ncomms2817.
39. Littlejohn, S.; Nogaret, A.; Crampin, S. *Adv. Mat.* **2011**, *23*, 2815-2818.

40. Maricich, S. M.; Wellnitz, S. A.; Nelson, A. M.; Lesniak, D. R.; Gerling, G. J.; Lumpkin, E. A.; Zoghbi, Merkel cells are essential for light-touch responses, *Science* **2009**, *324*, 1580.
41. Johnson, K. O.; Yoshioka, T.; Vega-Bermudez, F. tactile functions of mechanoreceptive afferents innervating the hand, *J. Clin. Neurophysiol.* **2000**, *17*, 539-558.
42. Burghard, M.; Klauk, H.; Kern, K. Carbon based field-effect transistors for nanoelectronics, *Adv. Mat*. **2009**, *21*, 2586-2600.
43. Kim, T.-I.; McCall, J. G.; Jung, Y. H.; Huang, X.; Siuda, E. R.; Li, Y.; Song, J.; Song, Y. M.; Pao, H. A.; Kim, R.-H.; Lu, C.; Lee, S. D.; Song, I.-S.; Shin, G.; Al-Hasani, R.; Kim, S.; Tan, M. P.; Huang, Y.; Omenetto, F. G.; Rogers, J. A.; Bruchas, M. R. Injectable, cellular scale optoelectronics with applications for wireless optogenetics, *Science* **2013**, *340*, 211-216.
44. Huang, J.-C. Carbon black filled conducting polymers and polymer blends, *Adv. Polym. Tech.* **2002**, *21*, 299-313.
45. Someya, T.; Sekitani, T.; Iba, S.; Kato, Y.; Kawaguchi, H.; Sakurai, T. A large-area, flexible pressure sensor matrix with organic field-effect transistors for artificial skin applications, *Proc. Nat. Acad. Sci.* **2004**, *101*, 9966-9970.
46. Pang, C.; Lee, G.-Y.; Kim, T.-I.; Kim, S. M.; Kim, H. N.; Ahn, S. –H.; Suh, K.-Y. A flexible and highly sensitive strain-gauge sensor using reversible interlocking of nanofibres, *Nature Mat.* **2012**, *11*, 795-801.
47. Dehé, A.; Fricke, K.; Mutamba, K.; Hartnagel, H. L.; A piezoresistive GaAs pressure sensor with GaAs/AlGaAs membrane technology, *J. Micromech Eng.* **1995**, *5*, 139-142.
48. Gad El Hak, M. The taming of the shrew: Why is it so difficult to control turbulence? *Act. Flow Control* **2007**, *95*, 1.
49. Fan, Z.; Ho, J. C.; Takahashi, T.; Yerushalmi, R.; Takei, K.; Ford, A. C.; Chueh, Y. –L.; Javey, A. Toward the development of printable nanowire electronics and sensors, *Adv. Mat*. **2009**, *21*, 3730-3743.
50. Sekitani, T.; Noguchi, Y.; Zschieschang, U.; Klauk, H.; Someya, T. Organic transistors manufactured using inkjet technology with subfemtoliter accuracy, *Proc. Nat. Acad. Sci.* **2008**, *105*, 4976-4980.
51. Berggren, M.; Nilsson, D.; Robinson, N. D. Organic materials for printed electronics, *Nature Mat*. **2007**, *6*, 3-5.
52. Garnier, F.; Hajlaoui, R.; Yassar, A.; Srivastava, P. All-polymer field-effect transistor realized by printing techniques, *Science* **1994**, *265*, 1684-1686.
53. Liao, W.-S.; Cheunkar, S.; Cao, H. H.; Bednar, H. R.; Weiss, P. S.; Andrews, A. M. Subtractive patterning via chemical lift-off lithography, *Science* **2012**, *337*, 1517-1521.
54. Stutzman, N.; Friend, R. H.; Sirringhaus, H. Self-aligned, vertical-channel, polymer field-effect transistors, *Science* **2003**, *299*, 1881-1884.
55. Liu, Y.; Weiss, D. N.; Li, J. Rapid nanoimprinting and excellent piezoresponse of polymeric ferroelectric nanostructures, *ACS Nano* **2010**, *4*, 83-90.
56. Hu, Z.; Tian, M.; Nysten, B.; Jonas, A. M. Regular arrays of highly ordered ferroelectric polymer nanostructures for non-volatile low-voltage memories, *Nature Mat.* **2009**, *8*, 62-67.
57. Weitz, R. T.; Ansharov, K.; Zschieschang, U.; Barrena Villas, E.; Goswami, D. K.; Burghard, M.; Dosch, H.; Jansen, M.; Kern, K.; Klauk, H. Organic n—channel transistors based on core-cyanated perylene carboxylic diimide derivatives, *J. Am. Chem. Soc.* **2008**, *130*, 4637-4645.

58. Zhang, J.; Feng, S.; Wang, X. DC current voltage characteristics of silicone rubber filled with conductive carbon black, *J. Appl. Polym. Sci.* **2004**, *94*, 587-592.
59. El-Kady, M. F.; Strong, V.; Dubin, S.; Kaner, R. B. Laser scribing of high-performance and flexible graphene-based electrochemical capacitors, *Science* **2012**, *335*, 1326-1330.
60. Di Ventra, M.; Pershin, Y. V.; Chua, L. O. Circuit elements with memory: Memristors, Memcapacitors and Meminductors, *Proc. IEEE* **2009**, *10*, 1717-1724.
61. Zou, J.-F.; Yu, Z.-Z.; Pan, Y.-X.; Fang, X.-P.; Ou, Y.-C. Conductive mechanism of polymer/ graphite conducting composites with low percolation threshold, *J. Polym. Sci. B* **2002**, *40*, 954-963.
62. Su, Q.; Pang, S.; Alijani, V.; Li, C.; Feng, X.; Müllen, K. Composites of graphene with large aromatic molecules, *Adv. Mat.* **2009**, *21*, 3191-3195.
63. Stankovich, S.; Dikin, D. A.; Dommett, G. H. B.; Kohlhaas, K. M.; Zimney, E. J.; Stach, E. A.; Piner, R. D.; Nguyen, S. T.; Ruoff, R. S. Graphene-based composite materials, *Nature* **2006**, *442*, 282-286.
64. Chen, Z.; Ren, W.; Gao, L.; Liu, B; Pei, S.; Cheng, H.-M. Three-dimensional flexible and conductive interconnected graphene networks grown by chemical vapour deposition, *Nature Mat.* **2011**, *10*, 424-428.
65. Lipomi, D. J.; Vosgueritchian, M.; Tee, B. C.-K.; Hellstrom, S. L.; Lee, J. A.; Fox, C. H.; Bao, Z. Skin-like pressure and strain sensors based on transparent elastic films of carbon nanotubes, *Nature Nanotech.* **2011**, *6*, 788-792.
66. Sekitani, T.; Nakajima, H.; Maeda, H.; Fukushima, T.; Aida, T.; Hata, K.; Someya, T. Stretchable active-matrix organic light-emitting diode display using printable elastic conductors, *Nature Mat.* **2009**, *8*, 494-499.
67. Wang, C.; Chien, J.-C.; Takei, K.; Takahashi, T.; Nah, J.; Niknejad, A. M.; Javey, A. Extremely bendable, high-performance integrated circuits using semiconducting carbon nanotube networks for digital, analog, and radio-frequency applications, *Nanoletters* **2012**, *12*, 1527-1533.
68. Chauhan, A. S.; Nogaret, A. Direct pressure sensing with carbon nanotubes grown in a micro-cavity, *Appl. Phys. Lett.* **102**, 233507 (2013).
69. Ramanathan, T.; Abdala, A. A.; Stankovich, S.; Dikin, D. A.; Herrera-Alonso, M.; Piner, R. D.; Adamson, D. H.; Schniepp, H. C.; Chen, X.; Ruoff, R. S.; Nguyen, S. T.; Aksay, I. A.; Prud'homme, R. K.; Brinson, L. C. Functionalized graphene sheets for polymer nanocomposites, *Nature Nanotech* **2008**, *3*, 327-331.
70. Zhang, X.; Pint, C. L.; Lee, M. H.; Schubert, B. E.; Jamshidi, A.; Takei, K.; Ko, H.; Gillies, A.; Bardhan, R.; Urban, J. J.; Wu, M.; Fearing, R.; Javey, A. Optically- and Thermally –responsive programmable materials based on carbon nanotube-hydrogel polymer composites, *Nanoletters* **2011**, *11*, 3239-3244.
71. Kim, D.-H.; Lu, N.; Ghaffari, R.; Kim, Y.-S.; Lee, S. P.; Xu, L.; Wu, J.; Kim, R.-H.; Song, J.; Liu, Z.; Viventi, J.; de Graff, B.; Elolampi, B.; Mansour, M.; Slepian, M. J.; Hwang, S.; Moss, J. D.; Won, S.-M.; Huang, Y.; Litt, B.; Rogers, J. A. Materials for multifunctional balloon catheters with capabilities in cardiac electrophysiological mapping and ablation therapy, *Nature Mat.* **2011**, *10*, 316-323.
72. Kim, R.-H.; Kim, S.; Song, Y. M.; Jeong, H.; Kim, T.-I.; Lee, J.; Li, X.; Choquette, K. D.; Rogers, J. A. Flexible vertical light emitting diodes, *Small* **2012**, *8*, 3123-3128.

73. Kim, R. -H.; Tao, H.; Kim, T.-I.; Zhang, Y.; Kim, S.; Panilaitis, B.; Yang, M.; Kim, D.-H.; Jung, Y. H.; Kim, B. H.; Li, Y.; Huang, Y.; Omenetto, F. G.; Rogers, J. A. Materials and designs for wirelessly powered implantable light-emitting systems, *Small* **2012**, *8*, 2812-2818.
74. Ahn, B. Y.; Duoss, E. B.; Motala, M. J.; Guo, X.; Park, S. –I.; Xiong, Y.; Yoon, J.; Nuzzo, R. G.; Rogers, J. A.; Lewis, J. A. Omnidirectional printing of flexible, stretchable and spanning silver microelectrodes, *Science* **2009**, *323*, 1590-1593.
75. Sekitani, T.; Takamiya, M.; Noguchi, Y.; Nakano, S.; Kato, Y.; Sakurai, T.; Someya, T. A large area wireless power transmission sheet using printed organic transistors and plastic MEMS switches, *Nature Mat.* **2007**, *6*, 413-417.
76. Tian, B.; Liu, J.; Dvir, T.; Jin, L.; Tsui, J. H.; Qing, Q.; Suo, Z.; Langer, R.; Kohane, D. S.; Lieber, C. M. Macroporous nanowire nanoelectronics scaffolds for synthetic tissues, *Nature Mat.* **2012**, *11*, 986-994.
77. Kim, D.-H; Viventi, J.; Amsden, J. J.; Xiao, J.; Vigeland, L.; Kim, Y.-S.; Blanco, J. A.; Panilaitis, B.; Frechette, E. S.; Contreras, D.; Kaplan, D. L.; Omenetto, F. G.; Huang, Y.; Hwang, K.-C.; Zakin, M. R.; Litt, B.; Rogers, J. A. Dissolvable films of silk fibroin for ultrathin conformable bio-integrated electronics, *Nature Mat.* **2010**, *9*, 511-517.
78. Hwang, S.-W.; Tao, H.; Kim, D.-H.; Cheng, H.; Song, J.-K.; Rill, E.; Brenckle, M. A.; Panilaitis, B.; Won, S. M.; Kim, Y.-S.; Song, Y. M.; Yu, K. J.; Ameen, A.; Li, R.; Su, Y.; Yang, M.; Kaplan, D. L.; Zakin, M. R.; Slepian, M. J.; Huang, Y.; Omenetto, F. G.; Rogers, J. A. A physically transient form of silicon electronics, *Science* **2012**, *337*, 1640-1644.
79. Xu, S.; Zhang, Y.; Cho, J.; Lee, J.; Huang, X.; Jia, L.; Fan, J. A.; Su, Y.; Su, J.; Zhang, H.; Cheng, H.; Lu, B.; Yu, C.; Chuang, C.; Kim, T.-I.; Song, T.; Shigeta, K.; Kang, S.; Dagdeviren, C.; Petrov, I.; Braun, P. V.; Huang, Y.; Paik, U.; Rogers, J. A. Stretchable batteries with self-similar serpentine interconnects and integrated wireless recharging systems, *Nature Comm.* **2013**, *4:1543*, 1-8.
80. Ko, H. C.; Shin, G.; Wang, S.; stoykovich, M. P.; Lee, J. W.; Kim, D.-H.; Ha, J. S.; Huang, Y.; Hwang, K.-C., Rogers J. A. Curvilinear electronics formed using silicon membrane circuits and elastomeric transfer elements, *Small* **2009**, *23*, 2703-2709.
81. Park, J. -U.; Nam, S. W.; Lee, M.-S.; Lieber, C. M. Synthesis of monolithic graphene-graphite integrated electronics, *Nature Mat.* **2012**, *11*, 120-125.
82. Esaki, L. New phenomenon in narrow germanium p-n junctions, *Phys. Rev.* **1957**, *109*, 603-603.
83. Tsu, R.; Esaki, L. Tunneling in a finite superlattice, *Appl. Phys. Lett*. **1973**, *22*, 562-564.
84. Chang, L.L.; Esaki, L.; Tsu, R. Resonant tunneling in semiconductor double barriers, *Appl. Phys. Lett*. **1974**, *24*, 593.
85. Eisenstein, J.P.; Pfeiffer, L.N.; West, K. W.; Coulomb barrier to tunneling between parallel 2-dimensional electron-systems, *Phys. Rev. Lett.* **1992**, *69*, 3804-3807.
86. Hayden, R. K.; Maude, D. K.; Eaves, L.; Valadares, E. C.; Henini, M.; Sheard, F.W.; Hughes, O.H.; Portal, J.C.; Cury, L. Probing the hole dispersion-curves of a quantum-well using resonant magnetotunneling spectroscopy, *Phys. Rev. Lett.* **1991**, *66*, 1749-1752.
87. Rascol, J.J.L.; Martin, K.P.; Carnahan, R.E.; Higgins, R.J.; Cury, L.A.; Portal, J.C.; Park, B.G.; Wolak, E.; Lear, K.L.; Harris, J.S. Influence of ballistic elelctrons on the device characteristics of vertically integrated resonant tunneling diodes, *Appl. Phys. Lett*. **1991**, *58*, 1482.

88. Wei S. –J.; Lin H. V. Multivalued SRAM cell using resonant tunneling diodes, IEEE J. *Solid State Circ.* **1992**, *27*, 212-216.
89. Van der Wagt J. P. A.; Seabaugh, A. C.; Beam III E. A. RTD/HFET low standby power SRAM gain cell, *IEEE Electron Dev. Lett.* **1998**, *19*, 7-9.
90. Gregor, L. V., Electrical conductivity of polydivinylbenzene films *Thin Solid Films* **1968**, *2*, 235-246.
91. Lauters, M.; McCarthy, B.; Sarid, D.; Jabbour, G. E. Multilevel conductance switching in polymer films, *Appl. Phys. Lett.* **2006***, 89*, 013507.
92. Bandyopadhyay, A.; Pal, A. J. Tuning of organic reversible switching via self-assembled supramolecular structures, *Adv. Mat.* **2003**, *15*, 1949.
93. Tseng, R. J.; Huang, J.; Ouyang, J.; Kaner, R. B.; Yang, Y. Polyaniline nanofiber/gold nanoparticle non-volatile memory, Nanolett. **2005**, *5*, 1077-1080.
94. Ma, L. P.; Liu, J.; Yang, Y. Organic electrical bistable devices and rewritable memory cells, *Appl. Phys. Lett*. **2002**, *80*, 2997-2999.
95. Ouyang, J.; Chu, C.-W.; Szmanda, C. R.; Ma, L.; Yang, Y. Programmable polymer thin film and non-volatile memory device, *Nature Mat.* **2004**, *3*, 918-922.
96. Möller, S.; Perlov, C.; Jackson, W.; Taussig, C.; Forrest, S. R. A polymer/semiconductor write-once-read-many-times memory, *Nature* **2003**, *426*, 166-169.
97. Möller, S.; Forrest, S. R.; Perlov, C.; Jackson, W.; Taussig, C. Electrochromic conductive polymer fuses for hybrid organic/inorganic semiconductor memories, *J. Appl. Phys*. **2003**, *94*, 7811-7819.
98. Marsman, A. W.; Hart, C. M.; Gelinck, G. H.; Geuns, T. C. T.; de Leeuw, D. M. Doped polyaniline polymer fuses: Electrically programmable read-only-memory elements, *J. Mater. Res.* **2004**, *19*, 2057-2060.
99. Taylor, D. M.; Mills, C. A. Memory effect in the current-voltage characteristic of a low-band gap conjugated polymer, *J. Appl. Phys.* **2001**, *90*, 306-309.
100. Ling, Q.; Shi, Y. S.; Ding, S. J.; Zhu, C.; Chan, D. S. H.; Kwong, D. –L.; Kang, E.-T.; Neoh, K.-G. Non-volatile polymer memory device based on a novel copolymer of N-vinylcarbazole and Eu-complexed vinylbenzoate, *Adv. Mat.* **2005**, *17*, 455.
101. Tseng, R. J.; Huang, J.; Ouyang, J.; Kaner, R. B.; Yang, Y. Polyaniline nanofiber/gold nanoparticle non-volatile memory, Nanolett. **2005**, *5*, 1077-1080.
102. Ma, D.; Aguiar, M.; Freire, J. A.; Hümmelgen, I. A. Organic reversible switching devices for memory applications, *Adv. Mat.* **2000**, 12, 1063-1066.
103. Vorotyntsev, M. A.; Skompska, M.; Pousson, E.; Goux, J.; Moise, C. Memory effects in functionalized polymer films: titamocene derivatized polypyrrole in contact with THF solutions, J. Electroanal. Chem. **2003**, *552*, 307-317.
104. Joo, W.-J.; Choi, T.-L.; Lee, J.; Lee, S.K.; Jung, M.-S.; Kim, N.; Kim, J. M. Metal filament growth in electrically conductive polymers for nonvolatile memory application, *J. Chem. Phys. B* **2006**, *110*, 23812-23816.
105. Ovshinsky, S. R.; Reversible electrical switching phenomena in disordered structures, *Phys. Rev. Lett.* **1968**, *21*, 1450.
106. Yang, J. J.; Pickett, M. D.; Li, X. M. Ohlberg, D. A. A.; Stewart D. R.; Williams, R. S. Memristive switching mechanism for metal/oxide/metal nanodevices, *Nature Nanotech.* **2008**, *7*, 429-433.

107. Choi, B. J.; Jeong, D. S.; Kim, S. K.; Rohde, C.; Choi, S.; Oh, J. H.; Kim, H. J.; Hwang, C. S.; Szot, K.; Waser, R.; Reichenberg, B.; Tiedke, S. Resistive switching mechanism of TiO_2 thin films grown by atomic layer deposition *J. Appl. Phys.* **2005**, *98*, 033715.
108. Alibart, F.; Pleutin, S.; Bichler, O.; Gamrat, C.; Serrano-Gotarredona, T.; Linares-Barranco, B.; Vuillaume, D. A memristive nanoparticle/organic hybrid synapstor for neuroinspired computing, *Adv. Func. Mat.* **2012**, *22*, 609-616.
109. Alibart, F.; Pleutin, S.; Guérin D.; Novembre, C.; Lenfant, S.; Lmimouni, K.; Gamrat, C.; Vuillaume, D. An organic nanoparticle transistor behaving as a biological spiking synapse, *Adv. Func. Mat.* **2010**, *20*, 330.
110. Jo, S. H.; Chang, T.; Ebong, I.; Bhadviya, B. B.; Mazumder, P.; Lu, W. Nanoscale memristor device as synapse in neuromorphic systems, *Nanolett.* **2010**, *10*, 1297-1301.
111. Bae S.; Kim, H.; Lee, Y.; Xu, X. F.; Park, J. S.; Zheng, Y.; Balakrishnan, J.; Lei, T.; Kim, H. R.; Song, Y. I.; Kim, Y. J.; Kim, K. S.; Ozyilmaz, B.; Ahn, J. H.; Hong, B. H.; Ijima, S. Roll-to-roll production of 30-inch graphene films for transparent electrodes, *Nature Nanotech*. **2010**, *5*, 574-578.
112. Lee, J.; Tao, L.; Hao, Y.; Ruoff, R. S.; Akinwande, D.; Embedded-gate graphene transistors for high-mobility detachable flexible nanoelectronics, *Appl. Phys. Lett.* **2012**, *100*, 152104.
113. Masum Habib, K. M.; Zahid F.; Lake, R. K. Negative differential resistance in bilayer graphene nanoribbons, *Appl. Phys. Lett.* **2011**, *98*, 192112.
114. McCann, E.; Fal'ko V. I. Landau-level degeneracy and quantum Hall effect in a graphite bilayer, *Phys. Rev. Lett.* **2006**, *96*, 086805.
115. McCann, E. Asymmetry gap in the electronic band structure of bilayer graphene, Phys. Rev. B **2006**, *74*, 161403.
116. Ohta, T.; Bostwick, A.; Seyller, T.; Horn, K.; Rotenberg, E. Controlling the electronic structure of bilayer graphene *Science* **2006**, *313*, 951**.**
117. Oostinga, J. B.; Heersche, H. B.; Liu, X.; Morpurgo, A. F.; Vandersypen, L. M. K. Gate-induced insulating state in bilayer graphene devices, *Nature Mat.* **2008**, *7*, 151-157.
118. Zhang, Y.; Tang, T.-T.; Girit, C.; Hao, Z.; Martin, M. C.; Zettl, A.; Crommie, M. F.; Shen, Y. R.; Wang, F. Direct observation of a widely tunable bandgap in bilayer graphene, *Nature* **2009**, *459*, 820-823.
119. Ren, H.; Li, Q.-X.; Yang, J. Graphene nanoribbon as a negative differential resistance device, *Appl. Phys. Lett.* **2009**, *94*, 173110.
120. Fang, H.; Wang, R.-Z.; Chen, S.-Y.; Yan, M.; Song, X.-M.; Wang, B. Strain-induced negative differential resistance in amchair-edge graphene nanoribbons, *Appl. Phys. Lett.* **2011**, *98*, 082108.
121. Iyengar, A.; Luo, T.; Fertig, H. A.; Brey, L. Conductance through graphene bends and polygons *Phys. Rev. B* **2008**, *78*, 235411.
122. Masir, M. R.; Vasilopoulos, P.; Peeters, F. M. Tunneling, conductance, and wavevector filtering through magnetic barriers in bilayer graphene, *Phys. Rev. B* **2009**, *79*, 035409.
123. Nguyen, V. H.; Bournel, A.; Nguyen, V. L.; Dolfus, P. Resonant tunneling and negative transconductance in single barrier bilayer graphene structure, *Appl. Phys. Lett.* **2009**, *95*, 232115.
124. Dresselhaus, M. S.; Dresselhaus, G. Intercalation compounds of graphite, *Adv. Phys.* **2002**, *51*, 1-186.

125. Grahn, H. T.; Haug, R. J.; Müller, W.; Ploog, K. Electric-field domains in semiconductor superlattices: A novel system for tunneling between 2D systems, *Phys. Rev. Lett.* **1991**, *67*, 1618-1621.
126. Zhang, J.; Zhang, S.; Feng, S.; Jiang, Z. The correlativity of positive temperature coefficient effects in conductive silicone rubber, *Polym. Int.* **2005**, *54*, 1175-1179.
127. Zhang, J.; Feng, D.; Feng, S.; Han, J.; Diao, G.; Liu, D. Correlation between current-voltage (I-V) characteristics in the electric-thermal equilibrium state and resistivity-temperature behavior of electro-conductive silicone rubber, *J. Appl. Polym. Sci.* **2008**, *107*, 2053-2057.
128. Wang, S.; Goh, B. M.; Manga, K. K.; Bao, Q.; Yang, P.; Loh, K.P. Graphene as atomic template and structural scaffold in the synthesis of graphene-organic hybrid wire with photovoltaic properties, *ACS Nano* **2010**, *4*, 6180-6186.
129. Pollard, A. J.; Perkins, E. W.; Smith, N. A.; Saywell, A.; Goretzki, G.; Phillips, A. G.; Argent, S. P.; Sachdev, H.; Müller, F.; Hüfner, S.; Gsell, S.; Fischer, M.; Schreck, M.; Osterwalder, J.; Greber, T.; Berner, S.; Champness, N. R.; Beton, P. H. Supramolecular assemblies formed on an epitaxial graphene superstructure, *Agnew Chem. Int. Ed.* **2010**, *49*, 1794-1799.
130. Chen, Q.; Zhang, X.; Chen, T.; Wang, D.; Qian, H.-L.; Wang, Z.-H.; Wan, L.-J. Substitution effect on the adlayer formation of tetrachloroperylene bismides on HOPG surface, *Surf. Sci.* **2010**, 604, 2078-2083.
131. Wang, Q. H.; Hersam, M. C. Nanofabrication of heteromolecular organic nanostructures on epitaxial graphene via room temperature feedback-controlled lithography, *Nanoletters*, **2011**, *11*, 589-593.
132. Kozlov, S. M.; Vines, F.; Görling, A. Bandgap engineering of graphene by physisorbed adsorbates, *Adv. Mat.* **2011**, *23*, 2638-2643.
133. Zhang, Z.; Huang, H.; Yang, X.; Zang, L. Tailoring electronic properties of graphene by π-π stcking with aromatic molecules, *J. Phys. Chem. Lett.* **2011**, *2*, 2897-2905.
134. Pengo, P.; Pantoş, G. D.; Otto, S.; Sanders, J. K. M. Efficient and mild microwave-assisted stepwise functionalization of naphthalenediimide with alpha aminoacids, *J. Org. Chem.* **2006**, *71*, 7063-7066.
135. Kleiner-Shuhler, L.; Brittain, R.; Johnston, M. R.; Hipps, K. W. Scanning tunneling microscopy and orbital-mediated tunneling spectroscopy of N, N' dioctyl naphthalenediimide adsorbed on highly ordered pyrolytic graphite, *J. Phys. Chem. C* **2008**, *112*, 14907-14912.
136. Timoschenko, S. Analysis of Bi-metal thermostats, *J. Opt. Soc. Am.* **1925**, *11*, 233-255.
137. Stoney, G. G. The tension of metallic films deposited by electrolysis, *Proc. Roy. Soc. Ser. A* **1909**, *82*, 172-175.
138. Rogers, J. A.; Someya, T.; Huang, Y. Materials and mechanics for stretchable electronics, *Science* **2010**, *327*, 1603-1607.

GRAPHICAL ABSTRACT